

OPEN ACCESS

EDITED BY

Yun Shen, Pennington Biomedical Research Center, United States

REVIEWED BY

Zhouyu Guan, Shanghai Jiao Tong University, China Yusen Li, The University of Chicago, United States

*CORRESPONDENCE Wenzhong Zhang

xxmczwz@qdu.edu.cn

[†]These authors have contributed equally to this work and share first authorship

RECEIVED 12 August 2025 ACCEPTED 13 October 2025 PUBLISHED 30 October 2025

CITATION

Li Z, Chen X, Ren L, Wang B, Ruan S, Wang J and Zhang W (2025) Explainable machine learning model for classifying atherosclerotic cardiovascular disease in patients with metabolic dysfunction-associated steatotic liver disease.

Front. Endocrinol. 16:1684558. doi: 10.3389/fendo.2025.1684558

COPYRIGHT

© 2025 Li, Chen, Ren, Wang, Ruan, Wang and Zhang. This is an open-access article distributed under the terms of the Creative Commons Attribution License (CC BY). The use, distribution or reproduction in other forums is permitted, provided the original author(s) and the copyright owner(s) are credited and that the original publication in this journal is cited, in accordance with accepted academic practice. No use, distribution or reproduction is permitted which does not comply with these terms.

Explainable machine learning model for classifying atherosclerotic cardiovascular disease in patients with metabolic dysfunction-associated steatotic liver disease

Zhengliang Li^{1†}, Xiaokai Chen^{2†}, Linlin Ren², Banghui Wang¹, Shimiao Ruan³, Juan Wang¹ and Wenzhong Zhang^{1*}

¹Department of Cardiology, The Affiliated Hospital of Qingdao University, Qingdao, Shandong, China, ²Department of Gastroenterology, The Affiliated Hospital of Qingdao University, Qingdao, Shandong, China, ³Department of Emergency, The Affiliated Hospital of Qingdao University, Qingdao, Shandong, China

Background: Cardiovascular disease (CVD) is the leading cause of mortality in patients with metabolic dysfunction-associated steatotic liver disease (MASLD), yet traditional risk predictors remain limited in clinical practice.

Objective: To develop machine learning (ML) models for classifying prevalent atherosclerotic cardiovascular disease (ASCVD) risk in MASLD patients, and to enhance model interpretability using SHapley Additive exPlanations (SHAP). Methods: This retrospective study included 590 MASLD patients diagnosed at the Affiliated Hospital of Qingdao University between December 2019 and December 2024. Patients were randomly divided into a training set (n=413) and a validation set (n=177), and further stratified based on ASCVD status. Least absolute shrinkage and selection operator (LASSO) regression was used for feature selection. Six ML models were developed and evaluated using sensitivity, specificity, accuracy, area under the receiver operating characteristic curve (AUC), and F1 score. SHAP analysis was performed to interpret feature contributions.

Results: ASCVD was present in 434 of 590 patients (73.6%). The Gradient Boosting (GB) model achieved the best performance, with AUCs of 0.918 (95% CI: 0.890–0.944) in the training set and 0.817 (95% CI: 0.739–0.883) in the validation set. SHAP analysis identified the top predictors as the Cholesterol–HDL–Glucose (CHG) index, Castelli Risk Index II (CRI-II), lipoprotein(a) [Lp(a)], serum creatinine (Scr), and uric acid (UA).

Conclusion: The GB model demonstrated strong high accuracy in identifying existing ASCVD in MASLD patients and may serve as a useful tool for early risk stratification in clinical settings.

KEYWORDS

metabolic dysfunction-associated steatotic liver disease, atherosclerotic cardiovascular disease, composite metabolic index, machine learning, SHAP interpretability model

1 Introduction

Non-alcoholic fatty liver disease (NAFLD) is a chronic metabolic stress-related liver disease that arises in genetically predisposed individuals due to overnutrition and insulin resistance (IR) (1). With the global rise in obesity and type 2 diabetes, the diagnostic criteria for this condition have undergone significant revisions. In 2020, an international expert panel proposed renaming the disease as metabolic dysfunction-associated fatty liver disease (MAFLD) (2), reflecting its underlying pathophysiology more accurately. In 2023, the European Association for the Study of the Liver (EASL) further updated the terminology to metabolic dysfunction-associated steatotic liver disease (MASLD), emphasizing the central role of metabolic and cardiovascular risk factors in its diagnosis (1). Recent epidemiological studies indicate that MASLD has become one of the most prevalent chronic liver diseases in China, with a continuously rising incidence (3).

Atherosclerotic cardiovascular disease (ASCVD) is one of the leading causes of death and disability worldwide (4–7). Its pathogenesis is closely linked to atherosclerosis and metabolic dysfunction. MASLD and ASCVD share multiple metabolic risk factors, and accumulating evidence suggests that the both presence and severity of MASLD are strongly associated with increased ASCVD risk (8, 9), Moreover, ASCVD is a major cause of mortality in patients with MASLD (10). Therefore, developing reliable and effective classification of prevalent ASCVD tools is critical for the early identification and intervention in individuals at high risk MASLD populations.

Currently, cardiovascular disease (CVD) risk assessment primarily relies on traditional indicators such as age, sex, smoking status, blood pressure, and high-density lipoprotein cholesterol (HDL-C) levels (11). Although widely used in clinical practice, these models have notable limitations. While HDL-C is a well-established inverse predictor of ASCVD events (12), its discriminative ability in identifying ASCVD among MASLD patients is limited. Such models often fail to account for the combined effects of dyslipidemia and impaired glucose regulation. In recent years, composite metabolic indices such as the cholesterol–HDL–glucose (CHG) index and Castelli's Risk Index II (CRI-II) have been proposed to better capture the impact of metabolic disturbances on cardiovascular risk (13).

Machine learning (ML), as an emerging modeling approach, offers strong capabilities in handling complex interactions and nonlinear relationships, and has been widely applied in the development of medical prediction models (14–17). For instance, Durán et al. (18) demonstrated nonlinear associations between gastric microbiota and proton pump inhibitor exposure, while Kha et al. (19) employed the Extreme Gradient Boosting (XGBoost) model to identify interactions among oral diabetes medications in patients with diabetes. Despite these powerful capabilities and increasing applications, a notable limitation of ML models remains their limited interpretability, often leading them to be characterized as "black box" models (20). SHapley Additive exPlanations (SHAP), a widely adopted interpretability

framework in recent years, improves model transparency and clinical acceptability by quantifying the contribution of each feature to the prediction output (21, 22).

Therefore, this study aimed to develop multiple ML models to identify existing ASCVD in patients with MASLD, and to incorporate the SHAP method for model interpretation, thereby providing an accurate, efficient, and interpretable tool to support clinical decision-making.

2 Methods

This study collected blood samples, basic medical history information, and ultrasound reports from patients, and conducted ML based on population characteristics to evaluate model performance and establish a model capable of effectively identifying MASLD patients at risk of ASCVD. The entire research workflow is summarized in Figure 1.

2.1 Study population

A total of 590 inpatients diagnosed with MASLD were retrospectively enrolled from the Affiliated Hospital of Qingdao University between December 2019 and December 2024. Written informed consent was obtained from all participants. The study protocol was approved by the Ethics Committee of the Affiliated Hospital of Qingdao University.

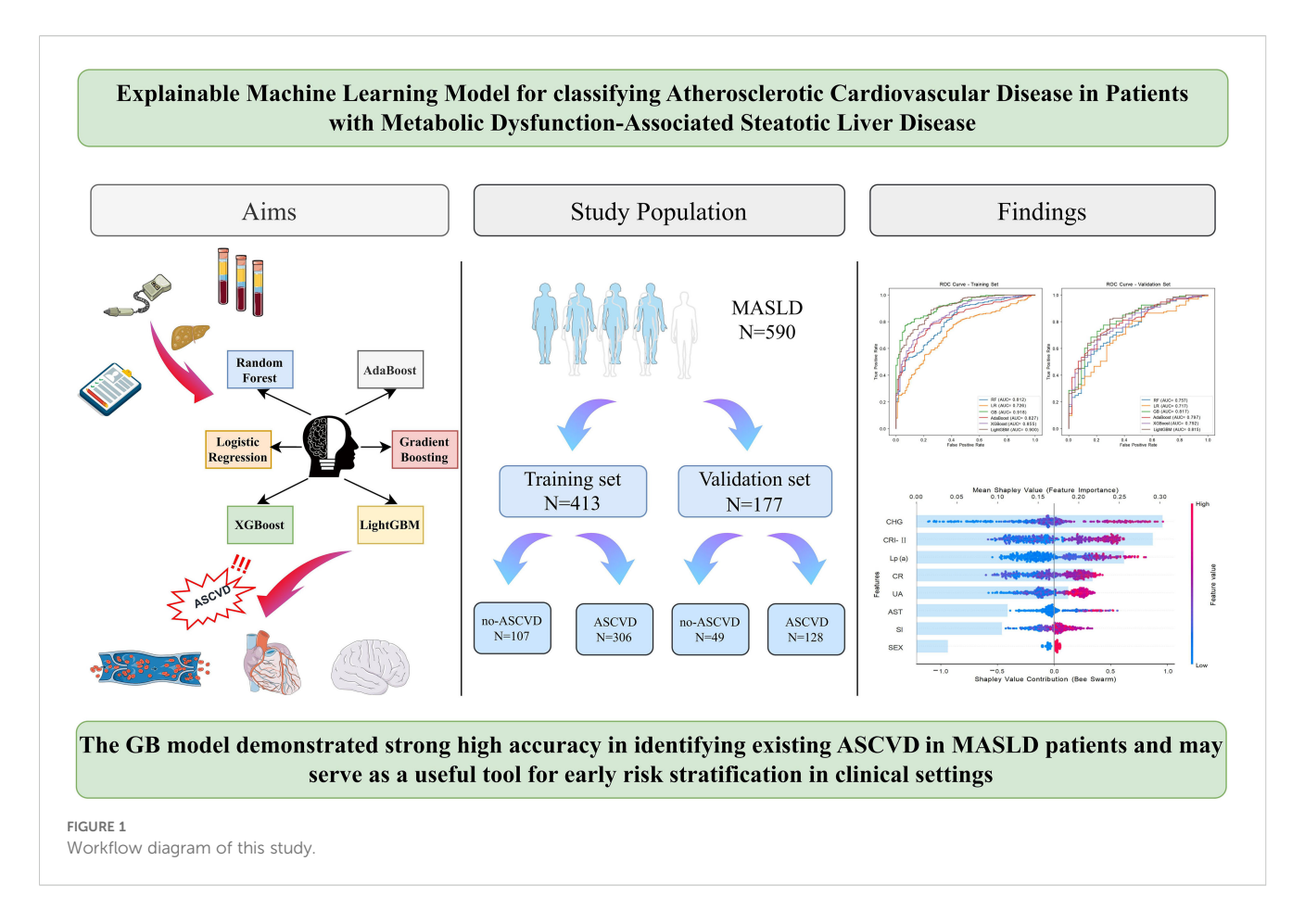
2.2 Inclusion and exclusion criteria

Inclusion criteria were as follows (1): Hepatic steatosis confirmed by standard abdominal ultrasonography (23). (2) Diagnosis of MASLD, defined as hepatic steatosis accompanied by at least one metabolic cardiovascular risk factor, including obesity, hypertension, prediabetes or a history of type 2 diabetes mellitus, hypertriglyceridemia, or low HDL-C levels.

Exclusion criteria included: (1) History of excessive alcohol consumption (≥140 g/week for men or ≥70 g/week for women); (2) History of viral hepatitis, liver cirrhosis, autoimmune liver disease, or drug-induced liver injury; (3) Use of antiplatelet or lipid-lowering medications; (4) History of coronary intervention or coronary artery bypass grafting (CABG); (5) Presence of other cardiac diseases;

(6) Severe renal insufficiency, malignancy, autoimmune disorders, acute or chronic infectious diseases, or major cerebrovascular disease.

The diagnosis of ASCVD was based on the 2013 ACC/AHA Guideline on the Treatment of Blood Cholesterol to Reduce Atherosclerotic Cardiovascular Risk in Adults (10), and included any of the following conditions: congestive heart failure, stable or unstable angina, acute myocardial infarction, ischemic stroke, or peripheral atherosclerosis.



2.3 Grouping method

All MASLD patients were classified into two groups based on the presence or absence of ASCVD: the MASLD-only group and the MASLD+ASCVD group. Subsequently, the entire cohort was randomly divided into a training set (n=413) and a validation set (n=177) in a 7:3 ratio for model development and validation.

2.4 Data collection and feature construction

Basic patient information was obtained from the electronic medical record system, including sex, age, height, weight, smoking and alcohol consumption history. Laboratory parameters included fasting blood glucose (FBG), alanine aminotransferase (ALT), aspartate aminotransferase (AST), triglycerides (TG), total cholesterol (TC), lipoprotein(a) [Lp(a)], HDL-C, low-density lipoprotein cholesterol (LDL-C), serum creatinine (Scr), cystatin C (CYSC), uric acid (UA), and blood cell count-related indices.

Based on the above data, several composite metabolic indicators were calculated to better reflect patients' metabolic status, including body mass index (BMI), sarcopenia index (SI), CHG index, Castelli's Risk Index I and II (CRI-I, CRI-II), atherosclerosis index (AIP), triglyceride–glucose (TyG) index, and the BMI-adjusted TyG index (TyG-BMI).

Data preprocessing and feature engineering were conducted in a Python 3.8 environment. The Pandas library (v1.3.3) was used for data loading, cleaning, and structural formatting. Numerical computation and missing value imputation were performed using NumPy (v1.21.2). Complete technical specifications are documented in Appendix A. To reduce feature dimensionality, enhance modeling efficiency, and control multicollinearity, least absolute shrinkage and selection operator (LASSO) regression with L1 regularization was applied for feature selection. The final feature set was determined exclusively by the LASSO regression without clinical judgment intervention. Ten-fold cross-validation was performed using the LassoCV module in the Scikit-learn library to automatically determine the optimal regularization parameter λ . Variables with non-zero coefficients were retained as input features for model construction. A regularization path plot illustrating coefficient shrinkage during LASSO selection was generated using Matplotlib (v3.4.3).

2.5 Machine learning model construction and hyperparameter optimization

After feature extraction and variable construction, six commonly used ML algorithms were developed based on the training set: Random Forest (RF), Logistic Regression (LR), Gradient Boosting (GB), Adaptive Boosting (AdaBoost),

XGBoost, and Light Gradient Boosting Machine (LightGBM) (24). The selection of the six machine learning approaches was guided by the following considerations: (a) Small-sample robustness: Treebased ensembles (RF, GB, AdaBoost, XGBoost, LightGBM) mitigate overfitting through regularization and ensemble mechanisms, while LR provides stable baselines for low-dimensional patterns; (b) Interpretability: LR enables direct coefficient interpretation, and tree-based models offer native feature importance outputs. (c) Computational efficiency: All ML demonstrate fast convergence on moderate-sized datasets, avoiding complex models requiring large-scale data (25, 26). Model development and training were conducted in a Python environment using mainstream open-source libraries, including Scikit-learn, XGBoost (v1.5.1), and LightGBM (v3.3.2).

To enhance model generalizability, all models were trained using a Pipeline framework combined with 10-fold cross-validation. Hyperparameter tuning was performed using the RandomizedSearchCV method. Model inputs were the key features selected via LASSO regression, and the output was a binary classification indicating the presence or absence of ASCVD.

To evaluate model performance, the following metrics were calculated on the validation set: area under the receiver operating characteristic curve (AUC), sensitivity, specificity, accuracy, positive predictive value (PPV), and F1 score. AUC was used as the primary indicator of discriminatory ability, while the F1 score was particularly emphasized to assess precision–recall trade-offs in the presence of class imbalance.

In addition, normalized confusion matrices were generated to visualize the classification ability of each model for positive and negative cases. Based on the overall performance across metrics, the best-performing model was selected for subsequent interpretability analysis.

Meanwhile, we selected the Prediction for ASCVD Risk in China (China-PAR project) model as the primary benchmark because it represents the current standard for ASCVD risk assessment in Chinese populations (27). It is important to note that while China-PAR was developed in general population cohorts, our study specifically targets the MASLD subpopulation.

2.6 Model interpretability analysis (SHAP)

To improve the transparency and interpretability of the machine learning model, SHAP was applied to the best-performing model for both global and individual-level interpretation. SHAP is based on the Shapley value concept from game theory and assigns each feature a contribution value for every individual prediction, thereby enabling transparent explanations of complex, nonlinear models.

At the global level, a SHAP feature importance plot was generated to rank the input variables according to their average absolute SHAP values, which reflect the mean magnitude of impact each feature has on the model's output. Higher values indicate greater overall influence on predictions.

A SHAP summary plot was then constructed to visualize how individual feature values contributed to model outputs across the entire dataset. Each point on the plot represents the SHAP value of a specific feature for one patient. The color gradient from red to blue indicates high to low feature values, while the distribution along the x-axis shows the direction and magnitude of each feature's effect on the prediction.

To further investigate nonlinear effects and feature interactions, SHAP dependence plots were generated. These plots visualize the marginal effects of predictors across their value ranges, revealing threshold effects and nonlinear relationships with prevalent ASCVD status.

At the individual level, SHAP force plots were created for two representative patients randomly selected from the cohort. These visualizations explain how each feature contributes to a specific prediction. In the force plots, red bars represent features that push the prediction toward the positive class (MASLD+ASCVD), while blue bars represent features that push it toward the negative class. The sum of these contributions, starting from the model's base value, yields the final predicted probability, illustrating a clear, feature-wise explanation path.

All SHAP analyses were performed in Python using the SHAP library (v0.40.0), with visualizations generated using Matplotlib and Plotly. The incorporation of SHAP not only enhanced model transparency but also provided valuable insights into high-risk features, thereby improving both clinical utility and model credibility.

2.7 Statistical analysis

All statistical analyses and visualizations were performed using R software (version 4.3.3) and SPSS software (version 27.0.0). Continuous variables were described as mean \pm standard deviation (SD) for normally distributed data, or as median with interquartile range (IQR) for non-normally distributed data. Categorical variables were expressed as counts (n) and percentages (%).

Comparisons between groups for categorical variables were conducted using the chi-square (χ^2) test. For continuous variables, independent samples t-tests were applied for normally distributed data, while nonparametric tests (e.g., Mann–Whitney U test) were used for skewed distributions. All statistical tests were two-sided, and a p-value < 0.05 was considered statistically significant.

3 Results

3.1 Comparison of baseline characteristics

A total of 590 patients with MASLD were enrolled in the study, including 413 cases assigned to the training set and 177 to the validation set. Within the training set, patients were further

stratified based on ASCVD status into the MASLD-only group (n = 107) and the MASLD+ASCVD group (n = 306).

Significant differences were observed between the two groups in several clinical and laboratory parameters. The MASLD+ASCVD group showed higher proportions of male patients and elevated levels of FBG, ALT, TG, TC, Lp(a), LDL-C, Scr, UA, CHG index, CRI-I, CRI-II, AIP, TyG, and TyG-BMI, all with statistically significant differences (p < 0.05). In contrast, HDL-C levels were significantly lower in the MASLD+ASCVD group than in the MASLD-only group (p < 0.05).

No statistically significant differences were observed in the remaining variables between the two groups (p > 0.05). A summary of baseline characteristics is presented in Table 1.

3.2 Feature selection results

A total of 25 clinical and biochemical variables were initially collected from the training dataset. To improve modeling efficiency, reduce redundancy, and minimize potential multicollinearity, we applied LASSO regression combined with 10-fold cross-validation for feature selection. As a result, eight variables with strong predictive value were retained (Figure 2): CHG, CRI-II, Lp(a), Scr, UA, AST, SI, and sex. These selected features were used in the subsequent modeling process, balancing predictive performance and model simplicity. The regularization path (Figure 2) illustrates the progressive shrinkage of variable coefficients as the regularization parameter (λ) increases.

3.3 Predictive performance of machine learning models

All six machine learning models demonstrated favorable predictive performance in both the training and validation cohorts. Among them, the GB model consistently outperformed others, achieving the highest AUC in both the training set (AUC = 0.918, 95% CI: 0.890–0.945) and validation set (AUC = 0.817, 95% CI: 0.739–0.883), as shown in Table 2 and Figure 3. In addition to AUC, the GB model also exhibited superior sensitivity (0.811), specificity (0.725), accuracy (0.785), and F1 score (Table 3, Figure 4), indicating its robust and balanced classification ability across multiple performance metrics.

Compared with Clinical Risk Scores, our model demonstrates superior performance in both the training set (AUC = 0.728, 95% CI: 0.674-0.780) and validation set (AUC = 0.724, 95% CI: 0.639-0.804) (Figure 5).

3.4 SHAP-based interpretation of the optimal model

To enhance the transparency and clinical interpretability of the machine learning model, SHAP analysis was applied to the best-performing GB model at both the global and individual levels.

At the global level, the SHAP feature importance plot (Figure 6A) identified CHG, CRI-II, Lp(a), Scr, and UA as the top five most influential predictors of ASCVD. The SHAP summary plot (Figure 6B) illustrated the direction and magnitude of each feature's contribution to the prediction outcome. Specifically, higher values of CHG, CRI-II, Lp(a), and UA were associated with greater positive SHAP values, indicating stronger driving forces toward predicting ASCVD. In addition, SHAP dependence plots (Figure 7) demonstrated a consistent positive marginal effect of these features on the model output, suggesting nonlinear trends and potential threshold effects.

At the individual level, force plots were generated for two representative patients—one correctly predicted as ASCVD-positive (true positive) and the other as ASCVD-negative (true negative) (Figures 8A, B). In these visualizations, red bars denote features that increase the prediction probability for ASCVD, while blue bars indicate features that decrease it. The length of each bar reflects the magnitude of contribution, and the final output is determined by the cumulative effect of all features starting from the model's base value. For instance, markedly elevated CHG and Lp(a) levels were major contributors to the ASCVD prediction, whereas higher HDL-C levels played a protective role.

In summary, the SHAP analysis not only confirmed the strong predictive value of key metabolic features in the GB model but also provided individualized explanations for model outputs. This highlights the model's potential utility in clinical decision support, offering both accurate prediction and interpretability.

4 Discussion

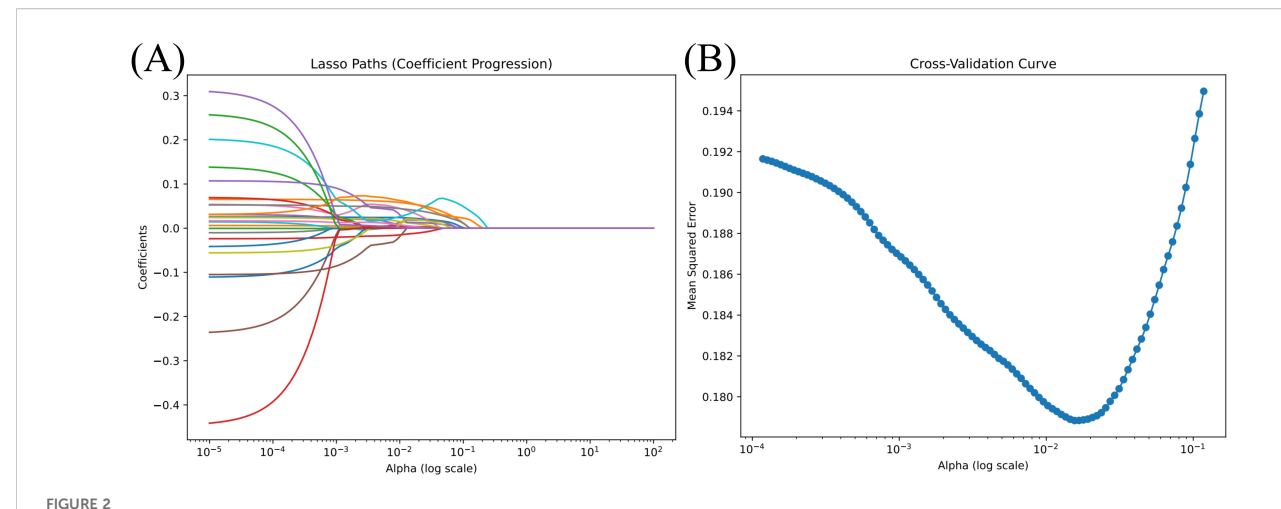
This study, based on real-world data from hospitalized MASLD patients, developed and compared multiple machine learning models to classify concurrent ASCVD. Eight key predictive features were identified through LASSO regression. The GB algorithm demonstrated superior predictive performance and stability within our cohort of hospitalized MASLD patients, with consistent results across both the training and validation sets. However, its relative advantage may vary across different clinical populations or with inclusion of additional features, underscoring the need for external validation to ensure broader applicability. Furthermore, the SHAP method was employed to enhance the interpretability and clinical transparency of the model.

MASLD and ASCVD share a wide range of metabolic risk factors. Our findings revealed that patients in the MASLD+ASCVD group exhibited significantly more severe abnormalities in metabolic indicators, indicating a substantial overlap between atherosclerotic risk and hepatic metabolic dysregulation. In the SHAP feature importance ranking, CHG, CRI-II, Lp(a), Scr, and UA emerged as the top contributors to the predictive model. These features reflect key metabolic mechanisms such as IR, dyslipidemia, renal dysfunction, and systemic inflammation, which are consistent with the established pathophysiology of both MASLD and ASCVD (8).

TABLE 1 Baseline characteristics of MASLD patients in the training and validation sets, stratified by ASCVD status.

	Trainin	Training set (n= 413)		Validatio	Validation set (n= 177)		۲
Characteristics	MASLD (n = 107)	MASLD+ ASCVD (n = 306)	p ¹ value	MASLD (n = 49)	MASLD+ ASCVD (n = 128)	p ² value	p ³ value
SEX, n (%)			0.017			0.27	0.067
Female	49 (45.8)	99 (32.4)		17 (34.7)	32 (25.0)		
Male	58 (54.2)	207 (67.6)		32 (65.3)	96 (75.0)		
SMOKE, n (%)			0.101			1	0.32
No	84 (78.5)	213 (69.6)		37 (75.5)	98 (76.6)		
Yes	23 (20.5)	93 (30.4)		12 (24.6)	30 (23.4)		
Fatty liver, n (%)			0.647			0.312	0.985
Grade 1	52 (48.6)	137 (44.8)		22 (44.9)	60 (46.9)		
Grade 2	47 (44.0)	138 (45.1)		20 (40.8)	59 (46.1)		
Grade 3	8 (7.4)	31 (10.1)		7 (14.3)	9 (7.0)		
Age (years)	63 (59, 69)	62 (54, 68)	0.062	63 (55, 68)	64 (57, 69)	0.475	0.356
Fib- 4	1.30 (1.01, 1.62)	1.29 (0.95, 1.81)	0.924	1.29 (0.93, 1.69)	1.39 (1.06, 2.02)	0.056	0.12
BMI (kg/m ²)	26.63 (24.79, 28.73)	26.99 (25.01, 29.07)	0.362	27.18 (24.91, 29.32)	26.27 (24.2, 28.74)	0.371	0.451
FBG (mg/dL)	102.42 (91.0, 117.72)	110.34 (95.76, 133.33)	0.003	106.56 (98.2, 119.7)	113.94 (95.3, 146.74)	0.34	0.211
AST (U/L)	20 (17, 25)	21 (17, 30)	0.055	21 (17, 26)	22 (18, 34)	0.096	0.313
ALT (U/L)	20 (15, 27)	24 (17, 34)	0.002	21 (18, 30)	25 (17, 37)	0.235	0.175
TG (mg/dL)	116.82 (90.71, 177.44)	145.14 (104.43, 198.24)	0.012	130.10 (94.69, 164.61)	136.29 (98.01, 204.44)	0.299	0.774
TC (mg/dL)	162.16 (127.03, 189.38)	174.13 (142.08, 207.14)	0.003	154.44 (131.27, 176.83)	174.90 (137.36, 210.91)	0.004	0.59
Lp (a) (mg/L)	107 (50, 202)	165 (64, 353)	0.002	115 (57, 237)	166.50 (75.75, 346.75)	0.089	0.911
HDL-C (mg/dL)	50.4 ± 9.6	48.1 ± 10.6	0.043	48.4 ± 11.7	48.6 ± 12.7	0.932	0.569
LDL-C (mg/dL)	84.69 (60.52, 105.18)	99.38 (72.41, 123.74)	< 0.001	81.21 (64.58, 102.48)	97.64 (70.77, 127.71)	0.003	0.762
Scr (mg/dL)	0.96 (0.87, 1.11)	1.03 (0.9, 1.18)	0.006	0.98 (0.83, 1.15)	1.07 (0.92, 1.17)	0.205	0.55
Cys-C (mg/dL)	0.09 (0.08, 0.11)	0.09 (0.08, 0.11)	0.203	0.09 (0.08, 0.11)	0.1 (0.08, 0.11)	0.09	0.451
PLT (10 ⁹ /L)	215 (187, 254)	223 (189, 267)	0.332	222 (177, 259)	223 (197, 256)	0.878	0.289
UA (umol/L)	330 (276.5, 390)	372.5 (306, 441.75)	< 0.001	349 (303, 408)	370.5 (310.25, 446.25)	0.178	0.261
SI	10.4 ± 2.6	10.8 ± 2.6	0.286	10.9 ± 2.9	10.6 ± 2.7	0.56	0.753
CHG	5.08 (4.88, 5.38)	5.31 (5.07, 5.61)	< 0.001	5.27 (4.91, 5.39)	5.39 (5.11, 5.72)	0.004	0.152
CRI-I	3.10 (2.74, 3.71)	3.72 (3.03, 4.37)	< 0.001	3.34 (2.82, 3.92)	3.74 (3.00, 4.46)	0.002	0.533
CRI-II	1.67 (1.29, 2.04)	2.12 (1.58, 2.67)	< 0.001	1.82 (1.34, 2.16)	2.09 (1.55, 2.76)	0.002	0.736
AIP	0.41 (0.23, 0.56)	0.47 (0.31, 0.65)	0.005	0.40 (0.29, 0.62)	0.44 (0.28, 0.67)	0.606	0.955
TyG	8.78 (8.39, 9.20)	9.01 (8.62, 9.40)	< 0.001	8.85 (8.47, 9.27)	9.05 (8.53, 9.48)	0.205	0.619
TyG-BMI	237.25 (216.37, 250.95)	243.72 (221.63, 267.56)	0.024	243.6 ± 35.5	243.2 ± 35.4	0.942	0.981

Data are presented as median (interquartile range, IQR), mean ± standard deviation (SD), or number (percentage), as appropriate. P^1 : P-value for comparison between MASLD and MASLD+ASCVD groups in the training set. P^2 : P-value for comparison between the training and validation sets (intergroup difference). Abbreviations: Fib-4, Fibrosis-4 index; BMI, body mass index; FBG, fasting blood glucose; AST, aspartate aminotransferase; ALT, alanine aminotransferase; TG, triglycerides; TC, total cholesterol; HDL-C, high-density lipoprotein cholesterol; Scr, serum creatinine; Cys-C, cystatin C; UA, uric acid; Plt, platelet count; SI, sarcopenia index; CHG, cholesterol-HDL-glucose index; CRI-I, Castelli's Risk Index II; AIP, atherogenic index of plasma; TyG, triglyceride-glucose index; TyG-BMI, BMI-adjusted TyG index.



Feature selection process using LASSO regression. (A) Coefficient shrinkage paths for all 25 candidate variables using least absolute shrinkage and selection operator (LASSO) regression. As the regularization parameter α (log scale) increases, less informative features are penalized and their coefficients shrink toward zero. (B) Ten-fold cross-validation curve showing the relationship between mean squared error (MSE) and α values. The optimal α , corresponding to the minimum MSE, was used to select the final subset of predictive features. This approach balances model simplicity and generalization performance. A total of 25 clinical and biochemical variables were entered into the model. Feature selection and visualization were performed using the LassoCV module from Scikit-learn (Python 3.8).

Traditional single lipid markers such as LDL-C have demonstrated limited effectiveness in early ASCVD classification of prevalent ASCVD (28). A previous study reported that approximately 77% of hospitalized ASCVD patients had LDL-C levels within the normal range (29), suggesting its insufficient standalone predictive value. In contrast, composite lipid indices such as CRI, AIP, and the TyG index, which simultaneously reflect multiple metabolic pathways, have shown superior performance in predicting cardiovascular and metabolic diseases (13, 30–32). Notably, this study is the first to systematically evaluate the CHG index for identifying ASCVD risk among MASLD patients, expanding its potential application in early metabolic risk management.

Unlike many prior "black-box" models, this study emphasized model interpretability. At the population level, SHAP feature rankings and dependence plots revealed the marginal and nonlinear effects of key variables. At the individual level, SHAP force plots provided transparent explanations of the prediction logic for specific patients, highlighting the positive or negative impact of each

variable. This approach offers valuable insight for developing transparent clinical decision support systems (CDSS).

Despite the promising findings, several limitations must be acknowledged. First, this study was conducted as a single-center retrospective analysis. The cohort was intentionally enriched with high-risk MASLD patients from tertiary hospital cardiology clinics, resulting in a higher observed ASCVD prevalence (73.6%) than population-based samples. While this design ensured adequate event rates for predictive modeling, it may introduce selection bias and limit external generalizability to community-based primary prevention settings. External validation in broader and more diverse cohorts is therefore warranted. Second, our outcome definition relied on administrative ICD codes (e.g., I50.x for heart failure), which cannot distinguish between atherosclerotic and nonatherosclerotic etiologies of congestive heart failure. Prospective studies with protocol-defined ASCVD adjudication are needed to confirm etiology-specific classifications. Third, although L1 regularization was used to mitigate overfitting, the relatively small sample size still poses a risk to the robustness of the conclusions.

TABLE 2 Predictive performance of six machine learning models in the validation cohort.

	AUC	Sensitivity	Specificity	Precision	F1 score
RF	0.757(0.675-0.839)	0.925(0.886-0.964)	0.364(0.293-0.435)	0.815(0.757-0.872)	0.866(0.816-0.916)
LR	0.717(0.633-0.796)	0.812(0.754-0.870)	0.477(0.404-0.551)	0.824(0.768-0.880)	0.818(0.761-0.875)
GB*	0.817(0.739-0.883)*	0.767(0.705-0.829)	0.750(0.686-0.814)	0.903(0.859-0.946)	0.829(0.774-0.885)
AdaBoost	0.797(0.720-0.865)	0.812(0.754-0.870)	0.568(0.495-0.641)	0.850(0.798-0.903)	0.831(0.776-0.886)
XGBoost	0.792(0.717-0.857)	0.759(0.696-0.822)	0.614(0.542-0.685)	0.856(0.804-0.908)	0.805(0.746-0.863)
LightGBM	0.815(0.743-0.881)	0.887(0.841-0.934)	0.500(0.426-0.574)	0.843(0.789-0.896)	0.864(0.814-0.915)

Values are expressed as mean (95% confidence interval). The Gradient Boosting (GB) model achieved the best overall performance, with the highest AUC and balanced sensitivity and specificity. F1-score is a metric synthesizing precision (proportion of positive predictions that are true) and recall (proportion of actual positives correctly predicted), balancing them to comprehensively reflect classification performance. AUC, area under the receiver operating characteristic curve; F1 score: harmonic mean of precision and recall; RF, random forest; LR, logistic regression; GB, gradient boosting; AdaBoost, adaptive boosting; XGBoost, extreme gradient boosting; LightGBM, light gradient boosting machine. "*" denotes highlighting that GB is the optimal model.

TABLE 3 Performance evaluation of the gradient boosting (GB) model in training and validation sets.

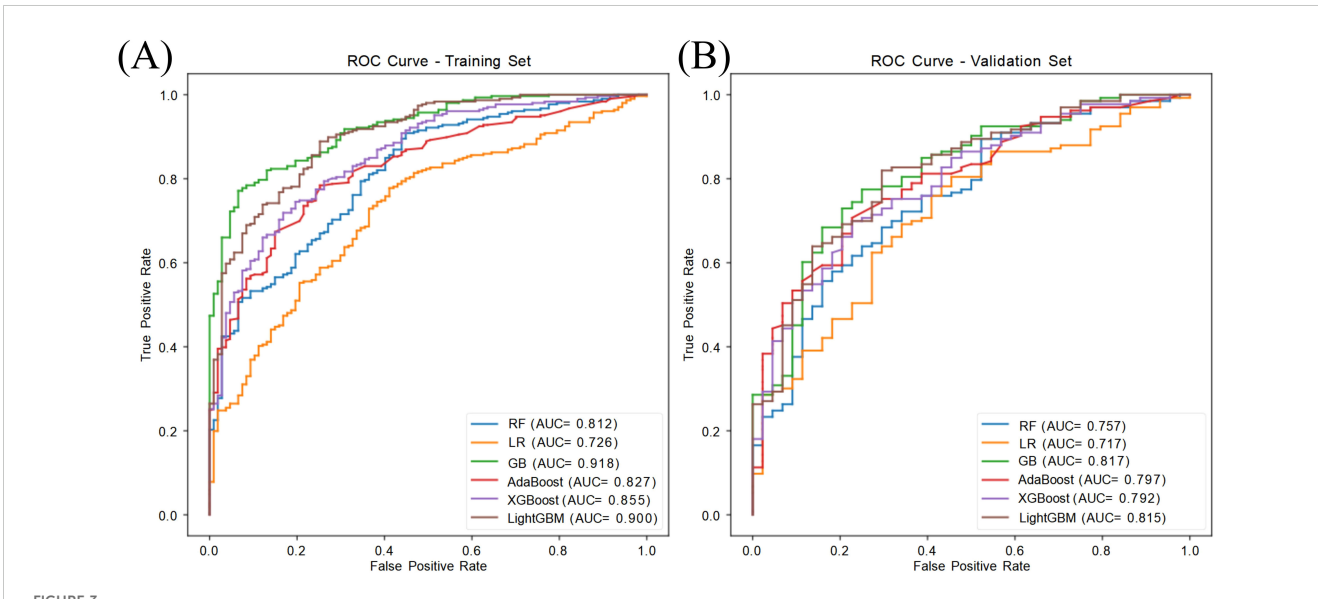
Metric	Training set (n=107/306)	Validation set (n=49/128)
AUC	0.918 (0.890-0.944)	0.817 (0.739-0.883)
Sensitivity	0.771(0.731-0.812)	0.767 (0.705-0.829)
Specificity	0.935(0.911-0.958)	0.750 (0.686-0.814)
Precision	0.971(0.955-0.987)	0.903 (0.859-0.946)
F1 score	0.860(0.826-0.893)	0.829 (0.774-0.885)

Model performance metrics for the Gradient Boosting (GB) algorithm were assessed in both the training set (n = 413; 306 positive, 107 negative) and validation set (n = 177; 128 positive, 49 negative). The GB model achieved an AUC of 0.918 in the training set and 0.817 in the validation set, with consistently high sensitivity, specificity, precision, and F1 score across both cohorts. Values are presented as point estimates with 95% confidence intervals in parentheses. Performance was evaluated based on five metrics: area under the receiver operating characteristic curve (AUC), sensitivity (recall), specificity, precision (positive predictive value), and F1 score (harmonic mean of precision and recall).

Fourth, the current model does not incorporate multimodal data such as imaging scores, genomic information, or lifestyle factors, which could further enhance predictive accuracy. Lastly, while SHAP-based explanations improve interpretability, further validation through mechanistic studies and clinical pathways is needed to confirm their clinical applicability and acceptance.

In conclusion, this study successfully developed a high-performing and interpretable classification model for identifying ASCVD in MASLD patients. By integrating machine learning with SHAP-based explanations, the model demonstrates strong potential for precision stratification and individualized risk assessment in metabolic diseases. The model demonstrates strong predictive performance in treatment-naive MASLD patients, providing a novel tool for early high-risk identification. While excluding lipid-lowering or antiplatelet therapy may limit immediate

generalizability to medicated populations, this approach helps preserves the integrity of metabolic risk drivers analysis. Importantly the key biomarkers highlighted by SHAP analysis—such as (e.g., Lp(a)—remain clinically actionable therapeutic targets for clinical intervention. The superior performance of our model compared to the China-PAR score underscores the value of a precision medicine approach for the distinct high-risk MASLD population. This difference likely stems from a fundamental divergence in design intent: while established scores like China-PAR are optimized for general population screening, our model is specifically engineered to capture the unique risk profile of MASLD patients. Therefore, our work provides a complementary, population-specific tool rather than a direct replacement for general-purpose scores, enabling more refined risk stratification for this cohort. Future work should focus on expanding to



ROC curves of six machine learning models in predicting ASCVD among MASLD patients. (A) Training set (n = 413); (B) Validation set (n = 177). Among all models, Gradient Boosting (GB) achieved the highest AUC in both sets (AUC = 0.918 in training, 0.817 in validation), indicating superior discriminative performance. Model performance was evaluated using 10-fold cross-validation and plotted with the ROC curve and AUC (95% CI). Abbreviations: RF, Random Forest; LR, Logistic Regression; GB, Gradient Boosting; AdaBoost, Adaptive Boosting; XGBoost, Extreme Gradient Boosting; LightGBM, Light Gradient Boosting Machine.

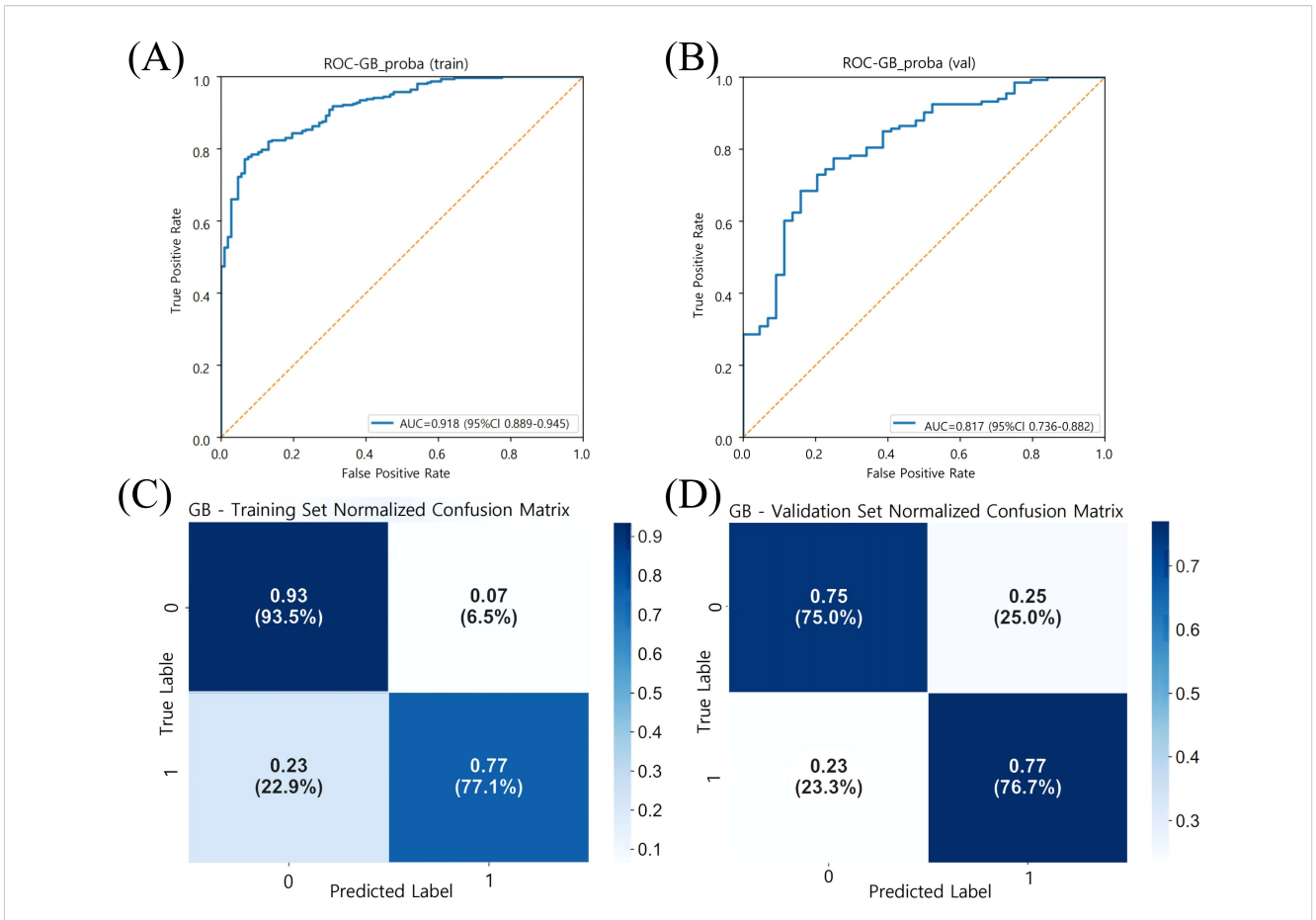
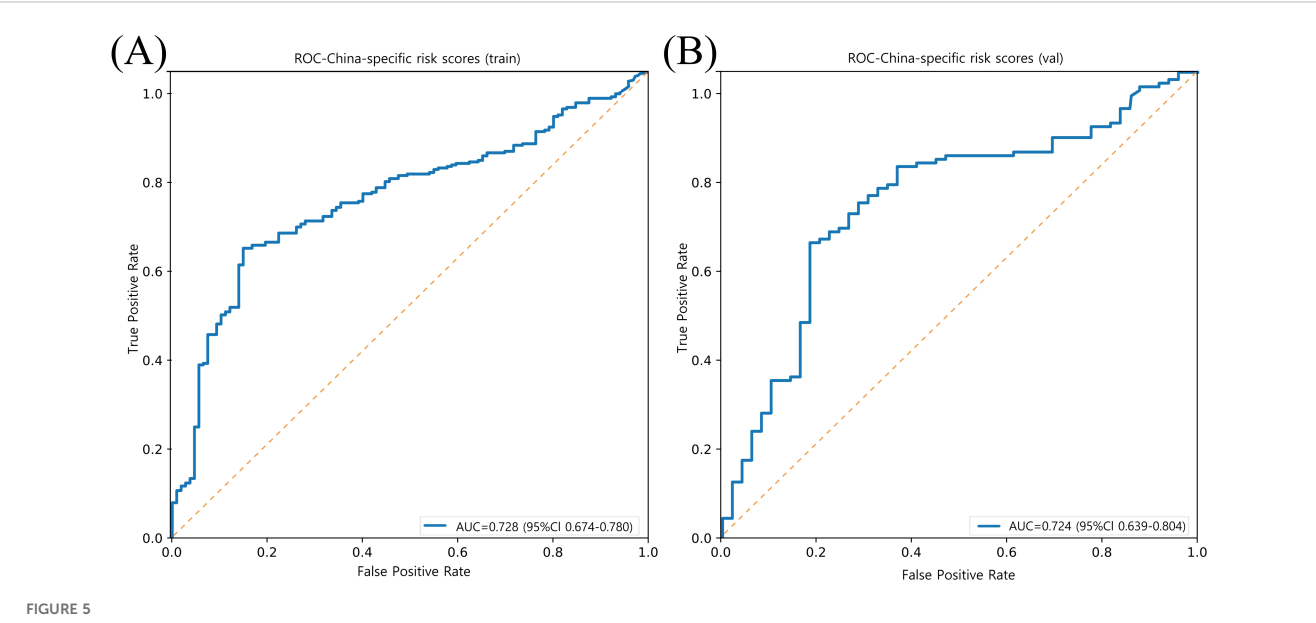
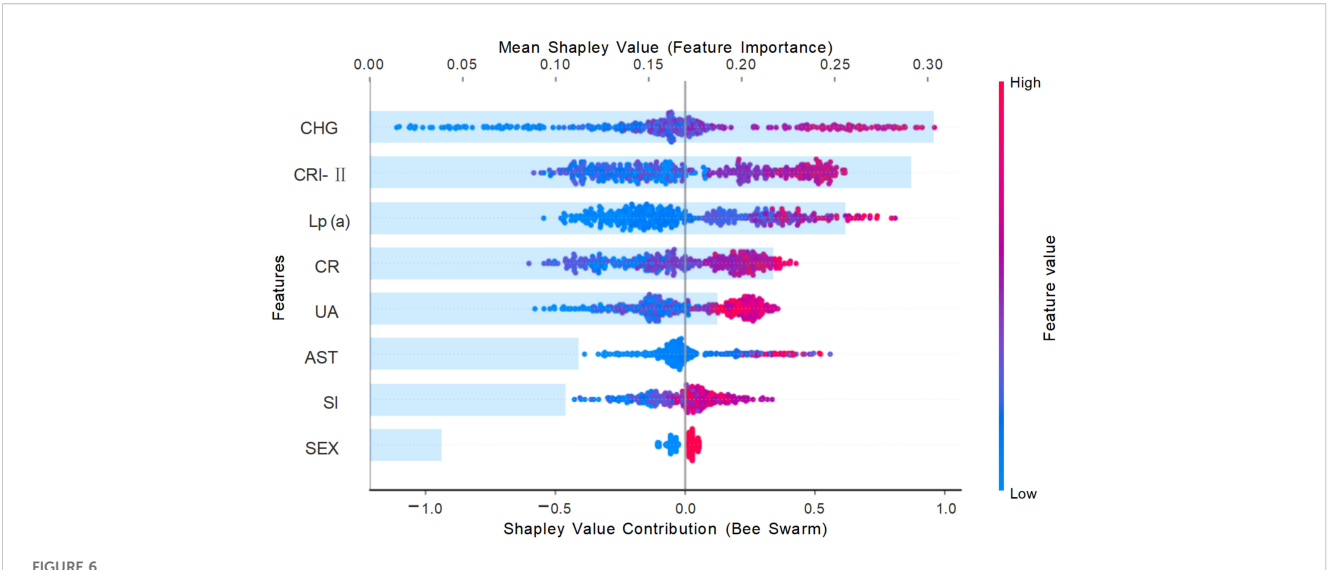


FIGURE 4 Model Performance of gradient boosting (GB) in training and validation sets. (A) ROC curve of the GB model in the training set (n = 413), with an AUC of 0.918 (95% CI: 0.890-0.945). (B) ROC curve of the GB model in the validation set (n = 177), with an AUC of 0.817 (95% CI: 0.739-0.883). The orange dashed line represents the no-discrimination reference line (AUC = 0.5). (C, D) Normalized confusion matrices of the GB model for the training and validation sets, respectively. Class 0: MASLD without ASCVD; Class 1: MASLD with ASCVD. Color intensity indicates normalized frequency. Model performance was evaluated using 10-fold cross-validation and reported using AUC, sensitivity, and specificity.



Model performance of prediction for ASCVD risk in China (China-PAR project) in training and validation sets. (A) ROC curve of the China-PAR project model in the training set (n = 413), with an AUC of 0.728 (95% CI: 0.674-0.780). (B) ROC curve of the China-PAR project model in the validation set (n = 177), with an AUC of 0.724 (95% CI: 0.639-0.804). The orange dashed line represents the no-discrimination reference line (AUC = 0.5).



Global feature importance based on SHAP values from the gradient boosting model Each dot represents an individual SHAP value for a feature in one patient. The x-axis indicates the direction and magnitude of the feature's impact on model output. Features are ranked by their mean absolute SHAP value. The color gradient (blue to red) represents low to high feature values. Features such as CHG, CRI-II, and Lp (a) show strong positive contributions to ASCVD risk prediction. SHAP values were derived from the Gradient Boosting model trained on the training set (n = 413), using the SHAP Python package (v0.40.0). Abbreviations: CHG, cholesterol-glucose index; CRI-II, Castelli risk index II; Lp(a), lipoprotein (a); CR, creatinine; UA, uric acid; AST, aspartate transaminase; SI, systolic index.

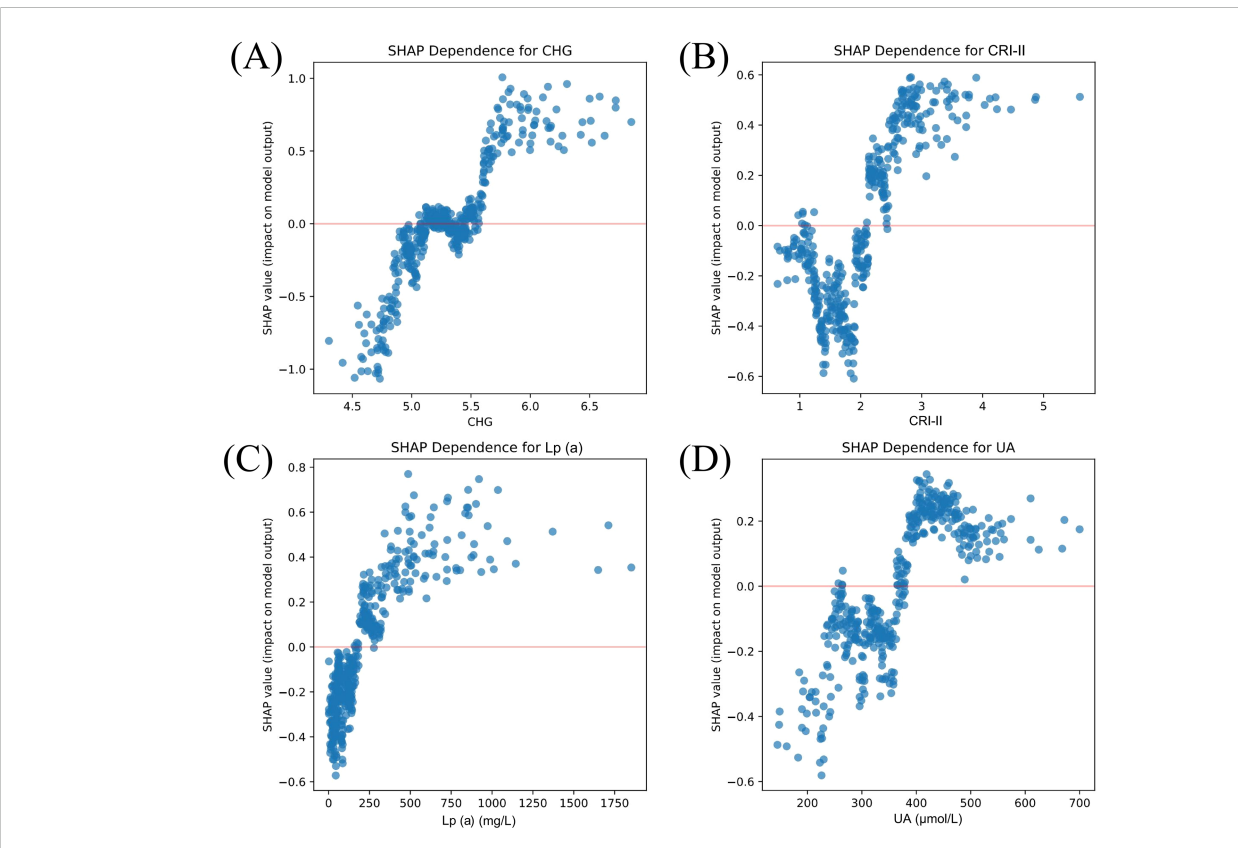
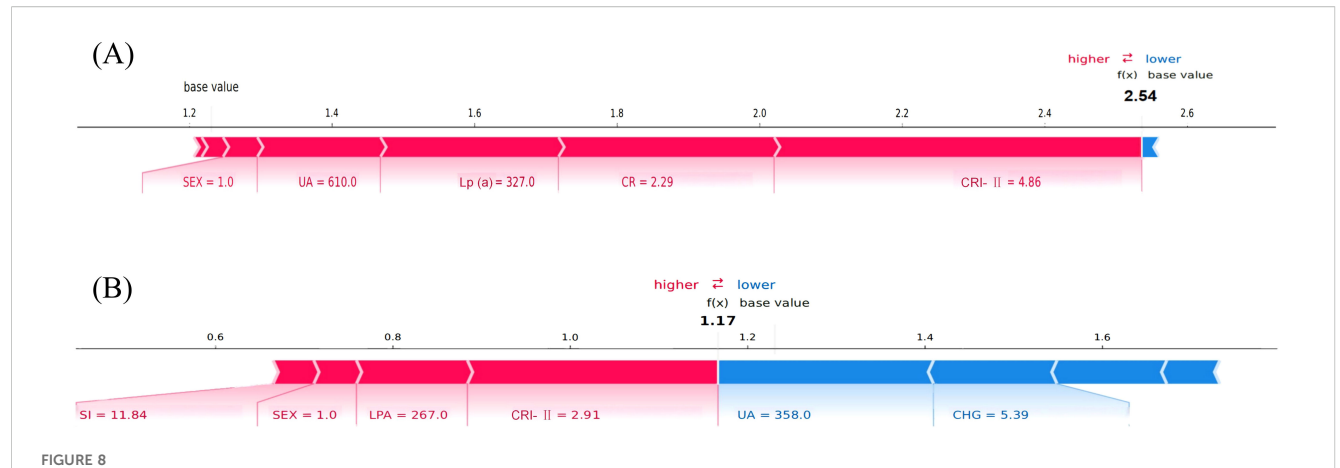


FIGURE 7
SHAP dependence plots of key predictive features SHapley Additive exPlanations (SHAP) dependence plots showing the marginal effects of the four most influential features on the prediction output of the Gradient Boosting model: (A) CHG, (B) CRI-II, (C) Lp(a), and (D) UA. The x-axis represents the actual value of each feature. The y-axis shows the corresponding SHAP value, indicating the direction and magnitude of that feature's contribution to the model prediction. Each dot corresponds to a single patient. These plots reveal nonlinear, positive associations between the feature values and their impact on ASCVD risk prediction, particularly highlighting threshold effects for CHG and Lp(a). The SHAP values were derived using the Gradient Boosting model trained on 413 patients in the training cohort, using the SHAP Python package (v0.40.0). CHG, cholesterol–glucose index; CRI-II, Castelli risk index II; Lp(a), lipoprotein (a); UA, uric acid.



SHAP force plots illustrating individual prediction explanations by the gradient boosting model. (A) Force plot for Patient A (true positive). The final model output f(x) = 2.54 exceeds the base value, indicating a high risk of ASCVD. (B) Force plot for Patient B (true negative). The output f(x) = 1.17 remains below the base value, suggesting no ASCVD. Red bars represent features that increase the predicted risk (positive contribution), while blue bars represent features that decrease it (negative contribution). The length of each bar indicates the magnitude of contribution. The grey vertical line represents the model's base value, i.e., the expected output when no features are present. SHAP (SHapley Additive exPlanations) values were calculated using the SHAP Python package (v0.40.0), based on the Gradient Boosting model trained on the training cohort (n = 413).

multicenter, multimodal datasets, conducting performance comparisons with traditional risk assessment models, developing integrated risk engines combining traditional factors with MASLD-specific biomarkers, and exploring the feasibility of clinical deployment to support personalized cardiovascular risk management in MASLD.

5 Conclusion

This study developed and validated multiple machine learning models to classify concurrent atherosclerotic cardiovascular disease (ASCVD) in hospitalized MASLD patients, using real-world cross-sectional data. Among the evaluated methods, tree-based ensemble learning algorithms—particularly Gradient Boosting—demonstrated the most robust performance in this specific cohort, showing high predictive accuracy and stability across both the training and validation sets. The eight high-value features selected via LASSO regression were also confirmed to have strong predictive contributions through SHAP interpretability analysis.

The innovation of this study lies in the integration of highperformance prediction modeling with interpretable machine learning, balancing accuracy with clinical applicability. In particular, the application of SHAP provided transparent decision-making support at both global and individual levels, enhancing the model's practical value in CDSS.

This model provides a novel tool for identifying MASLD patients with prevalent ASCVD, enabling individualized clinical assessment during hospitalization. Future work should focus on optimizing the model using multicenter datasets and expanding its scope by incorporating imaging, genetic, and behavioral data. This would provide a more comprehensive tool for early identification and intervention in MASLD patients at high risk for ASCVD.

Data availability statement

The original contributions presented in the study are included in the article/Supplementary Material. Further inquiries can be directed to the corresponding author.

Ethics statement

The study protocol was approved by the Ethics Committee of the Affiliated Hospital of Qingdao University. The studies were conducted in accordance with the local legislation and institutional requirements. The participants provided their written informed consent to participate in this study.

Author contributions

ZL: Conceptualization, Data curation, Writing – original draft, Writing – review & editing. XC: Investigation, Writing – original draft, Writing – review & editing. LR: Writing – original draft, Writing – review & editing. BW: Writing – original draft, Writing – review & editing. SR: Writing – original draft, Writing – review & editing. JW: Writing – original draft, Writing – review & editing. WZ: Data curation, Formal analysis, Writing – original draft, Writing – review & editing.

Funding

The author(s) declare that no financial support was received for the research and/or publication of this article.

Acknowledgments

Figure 1 was created using draw.io, with icons sourced from Unsplash (https://unsplash.com/) and Bioicons (https://bioicons.com/). All illustrations are used with permission. We acknowledge all individuals for their participation in this study.

Conflict of interest

The authors declare that the research was conducted in the absence of any commercial or financial relationships that could be construed as a potential conflict of interest.

Generative AI statement

The author(s) declare that no Generative AI was used in the creation of this manuscript.

Any alternative text (alt text) provided alongside figures in this article has been generated by Frontiers with the support of artificial

intelligence and reasonable efforts have been made to ensure accuracy, including review by the authors wherever possible. If you identify any issues, please contact us.

Publisher's note

All claims expressed in this article are solely those of the authors and do not necessarily represent those of their affiliated organizations, or those of the publisher, the editors and the reviewers. Any product that may be evaluated in this article, or claim that may be made by its manufacturer, is not guaranteed or endorsed by the publisher.

Supplementary material

The Supplementary Material for this article can be found online at: https://www.frontiersin.org/articles/10.3389/fendo.2025. 1684558/full#supplementary-material

References

- 1. European Association for the Study of the Liver (EASL)*, European Association for the Study of Diabetes (EASD) and European Association for the Study of Obesity (EASO). EASL-EASD-EASO Clinical Practice Guidelines on the management of metabolic dysfunction-associated steatotic liver disease (MASLD). *J Hepatol.* (2024) 81:492–542. doi: 10.1159/000539371
- 2. Eslam M, Newsome PN, Sarin SK, Anstee QM, Targher G, Romero-Gomez M, et al. A new definition for metabolic dysfunction-associated fatty liver disease: An international expert consensus statement. *J Hepatol.* (2020) 73:202–9. doi: 10.1016/j.jhep.2020.03.039
- 3. Yip TC, Fan JG, Wong VW. China's fatty liver crisis: A looming public health emergency. *Gastroenterology*. (2023) 165:825–7. doi: 10.1053/j.gastro.2023.06.008
- 4. GBD 2019 Diseases and Injuries Collaborators, et al. Global burden of 369 diseases and injuries in 204 countries and territories, 1990-2019: a systematic analysis for the Global Burden of Disease Study 2019. *Lancet.* (2020) 396:1204–22. doi: 10.1016/S0140-6736(20)30925-9
- 5. Xia X, Chen S, Tian X, Xu Q, Zhang Y, Zhang X, et al. Association of triglycerideglucose index and its related parameters with atherosclerotic cardiovascular disease: evidence from a 15-year follow-up of Kailuan cohort. *Cardiovasc Diabetol.* (2024) 23:208. doi: 10.1186/s12933-024-02290-3
- 6. Sandesara PB, Virani SS, Fazio S, Shapiro MD. The forgotten lipids: triglycerides, remnant cholesterol, and atherosclerotic cardiovascular disease risk. *Endocr Rev.* (2019) 40:537–57. doi: 10.1210/er.2018-00184
- 7. Wang F, Guo Y, Tang Y, Zhao S, Xuan K, Mao Z, et al. Combined assessment of stress hyperglycemia ratio and glycemic variability to predict all-cause mortality in critically ill patients with atherosclerotic cardiovascular diseases across different glucose metabolic states: an observational cohort study with machine learning. *Cardiovasc Diabetol.* (2025) 24:199. doi: 10.1186/s12933-025-02762-0
- 8. Chan WK, Chuah KH, Rajaram RB, Lim LL, Ratnasingam J, Vethakkan SR. Metabolic dysfunction-associated steatotic liver disease (MASLD): A state-of-the-art review. *J Obes Metab Syndr.* (2023) 32:197–213. doi: 10.7570/jomes23052
- 9. Driessen S, Francque SM, Anker SD, Castro Cabezas M, Grobbee DE, Tushuizen ME, et al. Metabolic dysfunction-associated steatotic liver disease and the heart. Hepatology. (2025) 82:487–503. doi: 10.1097/HEP.0000000000000735
- 10. Stone NJ, Robinson JG, Lichtenstein AH, Bairey Merz CN, Blum CB, Eckel RH, et al. 2013 ACC/AHA guideline on the treatment of blood cholesterol to reduce atherosclerotic cardiovascular risk in adults: a report of the American College of Cardiology/American Heart Association Task Force on Practice Guidelines. *Circulation*. (2014) 129:S1–45. doi: 10.1161/01.cir.0000437738.63853.7a
- 11. van Daalen KR, Zhang D, Kaptoge S, Paige E, Di Angelantonio E, Pennells L. Risk estimation for the primary prevention of cardiovascular disease: considerations for appropriate risk prediction model selection. *Lancet Glob Health*. (2024) 12:e1343–e58. doi: 10.1016/S2214-109X(24)00210-9

- 12. Barter P, Genest J. HDL cholesterol and ASCVD risk stratification: A debate. *Atherosclerosis.* (2019) 283:7–12. doi: 10.1016/j.atherosclerosis.2019.01.001
- 13. Mo D, Zhang P, Zhang M, Dai H, Guan J. Cholesterol, high-density lipoprotein, and glucose index versus triglyceride-glucose index in predicting cardiovascular disease risk: a cohort study. *Cardiovasc Diabetol.* (2025) 24:116. doi: 10.1186/s12933-025-02675-v
- 14. Stevens LM, Mortazavi BJ, Deo RC, Curtis L, Kao DP. Recommendations for reporting machine learning analyses in clinical research. *Circ Cardiovasc Qual Outcomes.* (2020) 13:e006556. doi: 10.1161/CIRCOUTCOMES.120.006556
- 15. Handelman GS, Kok HK, Chandra RV, Razavi AH, Lee MJ, Asadi H. eDoctor: machine learning and the future of medicine. *J Intern Med.* (2018) 284:603–19. doi: 10.1111/joim.12822
- 16. Ehrmann DE, Joshi S, Goodfellow SD, Mazwi ML, Eytan D. Making machine learning matter to clinicians: model actionability in medical decision-making. *NPJ Digit Med.* (2023) 6:7. doi: 10.1038/s41746-023-00753-7
- 17. Nohara Y, Matsumoto K, Soejima H, Nakashima N. Explanation of machine learning models using shapley additive explanation and application for real data in hospital. *Comput Methods Programs Biomed.* (2022) 214:106584. doi: 10.1016/j.cmpb.2021.106584
- 18. Durán C, Ciucci S, Palladini A, Ijaz UZ, Zippo AG, Sterbini FP, et al. Nonlinear machine learning pattern recognition and bacteria-metabolite multilayer network analysis of perturbed gastric microbiome. *Nat Commun*. (2021) 12:1926. doi: 10.1038/s41467-021-22135-x
- 19. Kha QH, Nguyen NTK, Le NQK, Kang JH. Development and validation of a machine learning model for predicting drug-drug interactions with oral diabetes medications. *Methods.* (2024) 232:81–8. doi: 10.1016/j.ymeth.2024.10.012
- 20. Giacobbe DR, Zhang Y, de la Fuente J. Explainable artificial intelligence and machine learning: novel approaches to face infectious diseases challenges. *Ann Med.* (2023) 55:2286336. doi: 10.1080/07853890.2023.2286336
- 21. Sylvester S, Sagehorn M, Gruber T, Atzmueller M, Schöne B. SHAP value-based ERP analysis (SHERPA): Increasing the sensitivity of EEG signals with explainable AI methods. *Behav Res Methods*. (2024) 56:6067–81. doi: 10.3758/s13428-023-02335-7
- 22. Ali S, Akhlaq F, Imran AS, Kastrati Z, Daudpota SM, Moosa M. The enlightening role of explainable artificial intelligence in medical & healthcare domains: A systematic literature review. *Comput Biol Med.* (2023) 166:107555. doi: 10.1016/j.compbiomed.2023.107555
- 23. Gofton C, Upendran Y, Zheng MH, George J. MAFLD: How is it different from NAFLD? Clin Mol Hepatol. (2023) 29:S17–s31. doi: 10.3350/cmh.2022.0367
- 24. Greener JG, Kandathil SM, Moffat L, Jones DT. A guide to machine learning for biologists. *Nat Rev Mol Cell Biol.* (2022) 23:40–55. doi: 10.1038/s41580-021-00407-0

25. Luo W, Phung D, Tran T, Gupta S, Rana S, Karmakar C, et al. Guidelines for developing and reporting machine learning predictive models in biomedical research: A multidisciplinary view. *J Med Internet Res.* (2016) 18:e323. doi: 10.2196/jmir.5870

- 26. Christodoulou E, Ma J, Collins GS, Steyerberg EW, Verbakel JY, Van Calster B. A systematic review shows no performance benefit of machine learning over logistic regression for clinical prediction models. *J Clin Epidemiol.* (2019) 110:12–22. doi: 10.1016/j.jclinepi.2019.02.004
- 27. Yang X, Li J, Hu D, Chen J, Li Y, Huang J, et al. Predicting the 10-year risks of atherosclerotic cardiovascular disease in chinese population: the China-PAR project (Prediction for ASCVD risk in China). *Circulation*. (2016) 134:1430–40. doi: 10.1161/CIRCULATIONAHA.116.022367
- 28. Farrell SW, Finley CE, Barlow CE, Willis BL, DeFina LF, Haskell WL, et al. Moderate to high levels of cardiorespiratory fitness attenuate the effects of triglyceride to high-density lipoprotein cholesterol ratio on coronary heart disease mortality in men. *Mayo Clin Proc.* (2017) 92:1763–71. doi: 10.1016/j.mayocp.2017.08.015
- 29. Sachdeva A, Cannon CP, Deedwania PC, Labresh KA, Smith SCJr., Dai D, et al. Lipid levels in patients hospitalized with coronary artery disease: an analysis of 136,905 hospitalizations in Get With The Guidelines. *Am Heart J.* (2009) 157:111–7.e2. doi: 10.1016/j.ahj.2008.08.010
- 30. Wang A, Tian X, Zuo Y, Chen S, Meng X, Wu S, et al. Change in triglyceride-glucose index predicts the risk of cardiovascular disease in the general population: a prospective cohort study. *Cardiovasc Diabetol.* (2021) 20:113. doi: 10.1186/s12933-021-01305-7
- 31. Lai H, Tu Y, Liao C, Zhang S, He L, Li J. Joint assessment of abdominal obesity and non-traditional lipid parameters for primary prevention of cardiometabolic multimorbidity: insights from the China health and retirement longitudinal study 2011-2018. *Cardiovasc Diabetol.* (2025) 24:109. doi: 10.1186/s12933-025-02667-y
- 32. Feng Y, Yin L, Huang H, Hu Y, Lin S. Assessing the impact of insulin resistance trajectories on cardiovascular disease risk using longitudinal targeted maximum likelihood estimation. *Cardiovasc Diabetol.* (2025) 24:112. doi: 10.1186/s12933-025-02651-6